

SFB 880 – EFFICIENT HIGH LIFT

J. Seume, S. Teichel, Institute of Turbomachinery and Fluid Dynamics
Leibniz Universität Hannover, Appelstr. 9, 30167 Hannover, Germany

M. Burnazzi, Institute of Fluid Mechanics, Technische Universität Braunschweig,
Hermann-Blenk-Str. 37, 38108 Braunschweig, Germany

M. Schwerter, Institute of Microtechnology, Technische Universität Braunschweig, Alte
Salzdahlumer Str. 203, 38124 Braunschweig, Germany

C. Behr, Institute of Adaptronics and Functional Integration, German Aerospace Center
(DLR), Langer Kamp 6, 38106 Braunschweig, Germany

A. Rudenko, Institute of Composite Structures and Adaptive Systems, German Aerospace
Center (DLR), Lilienthalplatz 7, 38108 Braunschweig, Germany

A. Schmitz, Institute of Aircraft Design and Lightweight Structures, Technische Universität
Braunschweig, Hermann-Blenk-Str. 35, 38108 Braunschweig, Germany

M. Dörbaum, Institute for Drive Systems and Power Electronics, Leibniz Universität
Hannover, Welfengarten 1, 30167 Hannover, Germany

Ç. Atalayer, Institute of Jet Propulsion and Turbomachinery, Technische Universität
Braunschweig, Hermann-Blenk-Str. 37, 38108 Braunschweig, Germany

Abstract

The collaborative research center (Sonderforschungsbereich, abbreviated SFB) 880 investigates the fundamentals of high-lift generation for future civil aircraft, focusing on the fields of aeroacoustics, lift generation and flight dynamics. The present paper addresses the research on efficient lift generation which is denoted as Research Area B.

The underlying research hypothesis of the present work is that further significant increases in lift generation of civil aircraft compared to the current state technology are possible using active lift systems. The investigated high-lift concept utilizes a combination of internally blown flaps and circulation control to achieve high flow turning over the wing. A flexible leading edge device for the wing without gap or step is designed to reduce noise generation and to increase the efficiency of the active blowing system. Further, closed-loop control of blowing is envisaged. The overall objective of the project is to design an active lift system that requires a minimum of additional engine power to generate the required lift. A multidisciplinary, collaborative approach is taken, combining the fields of aerodynamics, material science, microtechnology, turbomachinery and electrical engineering to obtain optimum performance of the overall lift generation system. The research progress during the first two years of this ongoing work is presented in this paper.

NOMENCLATURE

LGF	Lift Gain Factor
C_l	Lift Coefficient
C_μ	Momentum Coefficient
i	reference pressure
p_0	ambient pressure
α	Angle of Attack

1. INTRODUCTION

The motivation for this research lies in the conflict between the public desire towards faster and easier access to air travel on one hand and the resistance to air traffic related, noise and pollutant emission as well as the wasteful use of natural resources. Modern, efficient aircraft with short take-off and landing (STOL) capabilities are one way to approach this conflict. In this field of research the SFB 880 focuses on the fundamentals of aero acoustics and the use of porous materials to reduce noise, efficient lift

generation and the flight dynamics of aircraft with active lift systems. Aircrafts with active high lift systems are able to service airports with shorter runways thus improving the public access to air travel. High lift systems allow steeper take-off and landing trajectories decreasing the ground area that is exposed to aircraft related noise. The research approach on an efficient active lift system is presented in the following. Figure 1 illustrates the different aspects of the system that are investigated.

Preliminary studies have shown that an optimum leading edge shape, adapted for the momentary conditions of flight, has the potential to significantly increase the efficiency of the active blowing. The resulting reduction of momentum loss of the boundary layer directly upstream of the location, where active blowing is applied, reduces the required blowing rates and consequently increases efficiency of the high lift system.

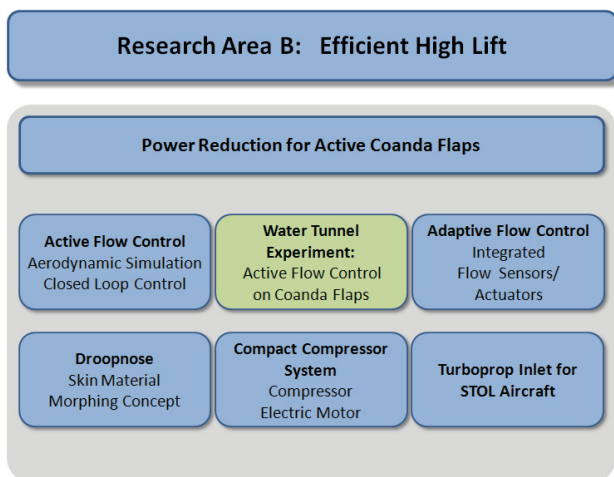
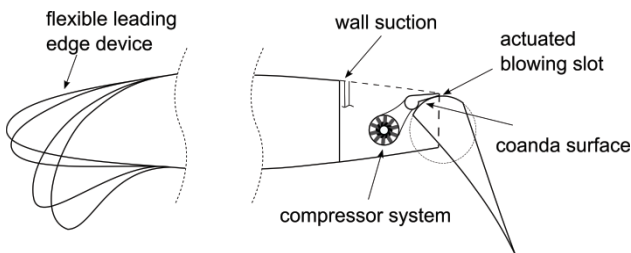


FIGURE 1. Fields of research of the active lift system.

The necessary deformation of the leading edge requires the development of new flexible skins of the wing, compliant mechanisms, and an appropriate design of the connection between the two. An optimization process is developed which provides the stiffness boundary conditions of the flexible skin and the topology of the compliant mechanism. To achieve high deformation in one direction and high stiffness of the flexible skin in span-wise direction, fiber composite materials are developed.

The blowing system uses electrically powered compressors located at each flap to provide the suction and the blowing mass flow rate. Single-stage axial compressors are chosen to cover the full operating range of this active lift system. High rotational speeds combined with large power demand are the challenges for the design of the electric motor. For the application in each flap of the wing, weight and compactness of the compressor system are critical design objectives.

The compressor system allows the use of synergetic effects between active blowing and boundary layer suction. The potential of this combined method is subject to current research.

Experimental validation of the numerical studies will be conducted with a scaled model in the water tunnel. To control the active blowing system, measuring and actuating elements are embedded in ductile polymeric material as part of the flexible wing structure. Prototypes of silicon-based pressure sensors and flexible hot wire anemometers for the application on cambered surfaces have been developed. The integration of these technologies in mechanically highly loaded systems will be tested for the application in an actuated blowing slot. Water Tunnel experiments are the basis of investigation of the high-lift system in regards of the aerodynamics of the lift generation and the adaptive flow control.

The high-lift system together with the goal of short take-off and landing capabilities of the investigated aircraft design require increased power of the turboprop engines. The turboprop engine design and in particular the design of the intake are investigated to account for propeller interaction, engine and the increased power.

The research done in the presented aspects of the active high lift system is presented in the following sections.

2. ACTIVE FLOW CONTROL

The efficiency of the active high-lift device is expressed by the Lift Gain Factor (LGF), which is defined as the ratio between the improvement of lift due to the high-lift system, divided by the momentum spent to obtain that gain:

$$\text{Lift Gain Factor} = \frac{\Delta C_{l,\max}}{C_{\mu}} \quad (1)$$

High Lift Gain Factors denote efficient active lift systems that generate lift with minimum momentum of the blowing jet. In Eqn. 1, $\Delta C_{l,\max}$ represents the gain in maximum lift coefficient and C_{μ} the momentum coefficient of the Coanda jet. Values of LGF around 80 have been achieved as a result of previous numerical and experimental work at the Technische Universität Braunschweig [1, 2, 3]. This work led to the design of a particular flap configuration which is used as a baseline in SFB 880 research. The following aerodynamic design approaches are used to further improve the Lift Gain Factor: (a) Gapless leading edge device to reduce boundary layer losses and also to yield low levels of airframe noise; (b) active circulation control using internally blown flaps and closed-loop flow control together with boundary layer suction: this approach promises large lift gains and it can be adapted to different operation points by flap setting.

The potentials of these research directions are initially investigated with numerical simulations. The numerical results are planned to be assessed experimentally by means of water-tunnel tests at high Reynolds numbers.

2.1. Gapless Leading Edge Device

The high circulation caused by a high-lift trailing-edge device generates a suction peak in the high curvature area of the leading-edge. As the angle of attack increases, the pressure gradient on the suction side grows rapidly. Therefore the improvement of lift allowed by the flap is

also associated with a significant reduction of the stall angle of attack. A suitable solution is the use of a leading-edge protection device, which adjusts the pressure distribution on the suction side of the airfoil. As a consequence of the increased stall angle of attack, also the maximum lift is considerably improved. Taking into account the low-noise requirements of the research project, a gap-less flexible droopnose shape has been designed. The shape of a fixed percentage of the chord length (which is the part of the airfoil not intersected by the wing box) was modified in order to reduce the suction peak and distribute the low pressure over a larger area. Initially, a rigid droop nose was also generated rotation of the nose around a hinge, located on the pressure side. In the final design, the camber and the thickness of the nose have been varied as morphed droopnose, which led to higher performances. Details about the droopnose design are presented in Ref. [4]. The new shape is intended for take-off and landing operations. Therefore an internal mechanism brings the airfoil back to the clean configuration during cruise conditions. The designed shapes and the performance improvements are shown in FIG. 2.

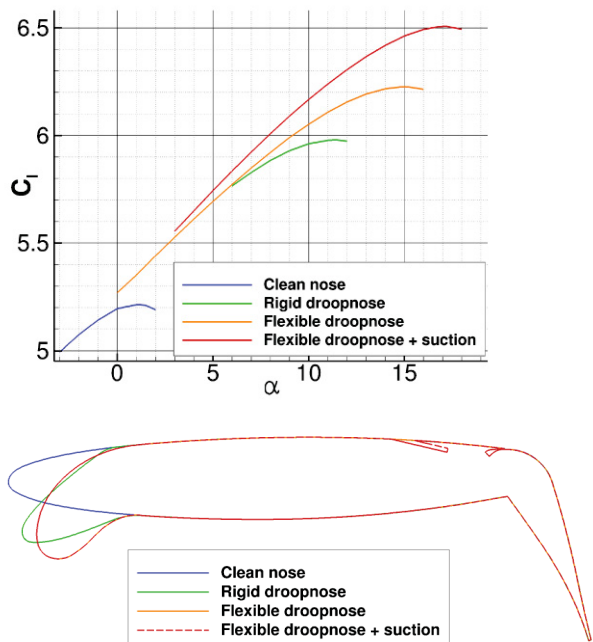


FIGURE 2. Lift coefficient vs. angle of attack for different airfoil configurations.

2.2. Boundary Layer Suction

The power needed to operate an active high-lift system is one of the most important issues for application in commercial aircraft. One approach is to rely on electrically-driven compact compressors, which are integrated along the wing span, behind the wingbox. These systems receive air from a slot positioned on the airfoil surface, and generate the wall jet needed to keep the flow attached to the Coanda surface of the flap. The wall suction represents an opportunity to further increase the aerodynamic performance of the airfoil. In fact, the momentum loss of the flow that reaches the Coanda jet, is critical for the efficiency of the active system to yield large flow turnings. Therefore, suction of the boundary layer upstream of the jet reduces the momentum requirement of the Coanda jet. On the other hand, the total pressure of

the air sucked from the wall is an important parameter for the compressor behavior and its power consumption. The position of the suction slot, as well as its internal shape are important for both the pressure recovery inside the duct and the stall performance of the airfoil. A sensitivity study of the internal duct shape showed that the improvement of the jet momentum achieved by a high total pressure at the end of the suction duct (considering a constant compression ratio of the compressor), dominates the overall gains expected from boundary layer suction. Taking into account the integration aspects of the suction system into the wing structure, the slot is positioned at 61% of the airfoil chord, which corresponds to the front edge of the spoiler, see FIGS. 1,2. However, different locations are also analyzed. As a consequence of the wall suction and the resulting improvement of the flow momentum over the blowing slot, a significant augmentation of both the maximum lift coefficient and the corresponding angle of attack is achieved.

2.3. Aerodynamic improvements

In FIG. 3 the evaluated performance of the airfoil configurations are summarized. Large improvement is achieved due to the well designed droopnose and the boundary layer suction, in comparison to the clean nose configuration. The effect of the droopnose appears to be significantly larger than the droopnose effect known with mechanical high-lift flaps. The benefit is to reduce the blowing power required by the Coanda flap and to increase the angle of attack of maximum lift coefficient. With the droopnose configuration the target $C_l \approx 4.7$ can be obtained with about 28% less jet momentum. Applying wall suction, a further reduction of 40% to the clean nose jet momentum is possible. As a consequence, the lift gain factor is increased by the same magnitude, reaching 114.5 for low blowing rates (Fig. 3). Note that the droopnose and suction concepts have so far been tested only for one flap setting with a deflection angle of 65°. Analysis performed with the clean nose configuration showed that higher lift gain factor may be achieved with a lower deflection, around 50°. It is concluded at this point that the performance of the droopnose and suction for other deflection angles than 65° remain to be seen.

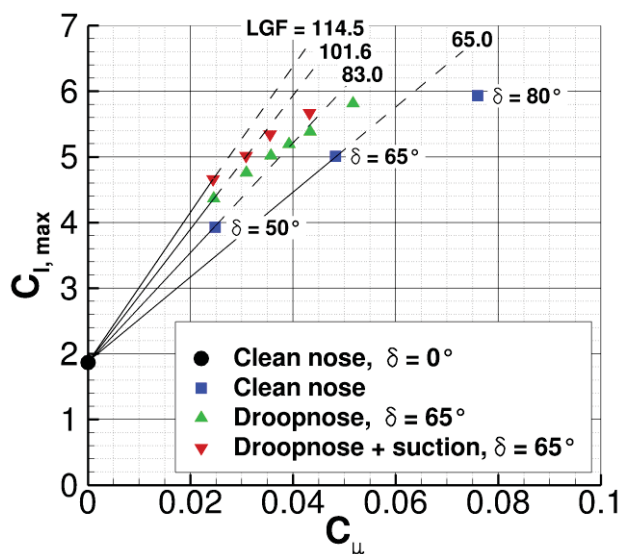


FIGURE 3. Lift coefficient vs. momentum coefficient for different airfoil configurations.

The pitching moment represents an important issue for the stability of the aircraft. With the current configuration, the load distribution along the chord is improved and the jet momentum requirement is decreased. This leads to an improvement in pitching moment by about 16% due to the droopnose configuration alone. Taking into account wall suction as well the pitching moment is improved by 33%.

The pitching moment represents an important issue for the stability of the aircraft. With the currently best configurations, the load distribution along the chord is improved and the jet momentum requirement is decreased. This leads to an improvement in pitching moment by about 16% due to the droopnose configuration alone. Taking into account wall suction as well the pitching moment is improved by 33%.

2.4. Closed-Loop Control

The use of pulsed blowing has been shown to increase the lift gains relative to the power expenditures needed to create the jet [5]. The balance between the power expended to generate the high speed jet and the lift gained can be further improved by employing a closed-loop control which controls the lift generation by regulating the blowing intensity. This process consists of acquiring flow data, computing the control variables, and acting on the flow accordingly. For that purpose a reduced-order model of the flow has to be created, based on a reduced physical model. This model needs to capture the governing physics by concentrating on the most important structures in the flow but also needs to be simple enough to be computed in real time.

The common approach is the use of a Galerkin model based on proper orthogonal decomposition (POD), which fulfills those requirements. The POD, based on a time resolved database of the flow, decomposes the flow into a series of spatial modes and their corresponding time coefficients with decreasing total kinetic energy. The Galerkin projection then produces a low-order system of ordinary differential equations which describe the evolution of the time-coefficients. Therefore the entire flow-field is described by projection of the governing equations onto the subspace spanned by the POD modes. It is assumed that the controlled flow varies between two states, the natural unactuated and the actuated state. Both can be modeled by using just the first few modes containing more than 95% of the total kinetic energy. One method to describe two operating conditions in a single approach consists of adding a shift-mode [7, 8]. The shift-mode constitutes the orthonormalized mean-field correction, capturing the difference between the actuated and the non actuated solutions.

POD Galerkin models have been extensively studied, and were shown capable of representing and controlling several flow problems [8]. However, those models were based on DNS data that resolves the flow down to the smallest scales. When uRANS simulations are used to obtain the time-resolved database of the flow simulation, the Galerkin POD model can become unstable due to the unresolved dissipative small scales in the flow simulation. A common approach to alleviate the problem is to calibrate the model by adding an eddy viscosity term. This technique and other calibration methods are detailed in Cordier et al. [9]. Model calibration improves the model behavior significantly but does not guarantee its stability, especially for time periods beyond the training phase. Alternatively, a modified Galerkin model, as introduced by Luchtenburg et al. [7], is being tested. It is a simplified

version of the original POD-Galerkin model, but is inherently more stable. For flow control, it is imperative that the reduced-order model is able to predict all significant flow conditions. Therefore, further development of the model to include transient and actuation modes is required. With a flexible model, the control systems and actuation response can then be tested using numerical simulations and the water tunnel experiment.

2.5. Water Tunnel Experiments

Experimental testing of a 2D-model of a Coanda-airfoil is currently in progress of work. These tests are used to validate the high-lift concept with droop-nose and a controlled Coanda jet, utilizing the developed sensor and actuator concepts presented in Sec. 3. The experimental setup is also used to generate an experimental database for the model-building process.

The tests will be carried out in the water-tunnel because of the advantage of high Reynolds-number at low flow velocity. Due to this low flow velocity compared to wind-tunnel testing, time-resolved measurements of the Coanda airfoils are possible in the water-tunnel. The flow field around the airfoil and especially behind the flap will be measured with a high-speed PIV-system. This information can then be used to feed the model-building process with experimental data and compare the resulting models with those built on numerical simulations. Numerical studies have shown better performance of the airfoil by adding a droopnose. Therefore this geometry has been chosen for the water tunnel model. The model has a span of 1000 mm and a chord length of 300 mm, allowing for a maximum Reynolds number of 3 million. The flap is deflected by 65°, the Coanda slot above the flap is formed by a replaceable lip. The model is equipped with 60 pressure taps for static and partly unsteady measurements and a hot-film array on the flap. Two measurement campaigns are planned. In the first campaign, the model is equipped with a non-actuated dummy-lip to gather data for the reference case of static blowing. The second campaign will be performed with an actuated lip which should bring new insight on the increased efficiency of pulsed blowing. Both campaigns will also provide time-resolved data of pressure and shear-stress on the flap to improve the model-building by providing feedback information to the model. The actuated lip also contains miniaturized pressure and shear-stress sensors to obtain further time-resolved information on the flow upstream the Coanda-slot.

3. ADAPTIVE FLOW CONTROL

The methods used to investigate the physical principle of active lift generation and to deduce a model suitable for closed-loop control are presented in the previous sections. Other critical components of the closed-loop control are the ability to determine the current state of the flow via measurement and the control of the blowing conditions.

Active flow control via actuated airfoils enables new approaches for future aircraft. Hereby the combination of micro electro mechanical sensor (MEMS) based on flow sensors and piezoelectric actuators were determined as a promising solution. These techniques will be integrated in a fiber composite lamination process in order to manufacture innovative, large-area sensor-actuator-arrays. Sensor and actuator designs are tailored satisfy

the requirements imposed by mechanical and aerodynamic constraints. The developed technologies will be demonstrated for the application of an oscillating lip of a blowing slot. These flow investigations will be performed in the water tunnel because the flow velocity and system's control frequency can be reduced due to the achievable high Reynolds numbers in the water tunnel compared to a wind tunnel. The airfoil model for water tunnel testing is schematically shown in FIG. 4. The design of the actuated lip is based on a FEM analysis. A piezo ceramic d33-stack actuator, operating at low voltage levels is being elaborated as an adequate actuation system. In a first functional demonstrator the actuators are embedded in a metal substrate as a bending actuator for basic experiments in the water tunnel. Preliminary mechanical tests serve as FEM model validation and are a measure of attainable nominal displacement and blocking force of the actuated lip. The evaluation of these tests indicates that the required slot height of 0.2 mm can be achieved with the developed design. A waterproof coating for the piezoelectric actuators for the application in the water tunnel is in development.

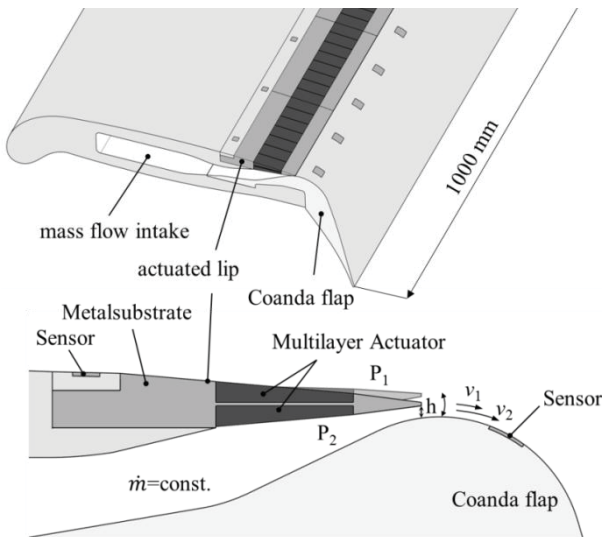


FIGURE 4. Concept of the actuated slot-lip for water tunnel tests.

A MEMS concept suitable for flow analyses on airfoils is developed. Thereby airflow disruption at a high lift configuration is to be detected. A non-intrusive measuring system is developed considering limitations regarding size, weight and power consumption. Having information about pressure and velocity above the wing surface the additional air jet needed for high lift operation can be controlled by an actuated lip.

As a suitable system a piezoresistive, silicon based pressure sensor is identified, being developed for basic experiments in the water tunnel. Herein the robustness, the high frequency capability and the achievable accuracy are the key criteria. In parallel, hot-film anemometers on flexible foils are developed to analyze the state of the flow on a strongly curved high-lift flap. In order to reduce space an integration of both sensors is desired. Therewith the pressure and the state of the flow can be measured at nearly the same point. Additionally an electrical circuit for digitizing the sensor's outputs is part of the overall system. This circuit is inserted in the new wing design in a way which complies with the measurement requirements and

the dimensions of the measured system. The requirements following out of the intended use for closed-loop control are considered in the design of the sensing system. Numerical investigations indicate that an actuation frequency of 300 Hz is required. Therefore the sensing system has to operate with 3 kHz at minimum. Both pressure and hot-film anemometer sensors were developed and fabricated as separate units to reduce the fabrication complexity.

The pressure sensor is a micro system with an overall dimension of 6.5 x 6.5 x 0.86 mm. During fabrication, many different microtechnological process steps are performed, for example lithography, diffusion, deposition and etching.

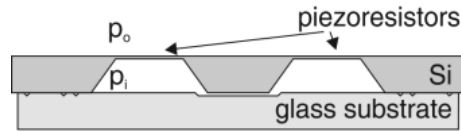


FIGURE 5. Cross sectional sketch of the piezoresistive pressure sensor

As shown in FIG. 5, the pressure sensor is realized in silicon with piezoresistors within its membrane. A cavity is filled with nitrogen with the reference pressure p_i . Having a difference between the ambient pressure p_o and p_i the membrane deflects which leads to stresses in the membrane and hence to resistance change in the piezoresistors. The piezoresistors are connected to a Wheatstone bridge to avoid temperature influences and to reach a higher sensitivity. The sensitivity strongly depends on the deflection availability of the membrane. Hence a simulation was done to calculate the thinnest possible membrane withstanding all forces expected to occur. Additionally, the simulation reveals the membrane's edges as optimal positions for the piezoresistors [10]. The output signal of the sensor is in the two-digit millivolt range when applying three volts on the Wheatstone bridge. This signal is amplified and digitized. To comply with the limitations in size and to achieve electromagnetic compatibility, the digitizing electronic is located directly besides the sensor. A shift-register system outputs the signal of all sensors serially to the closed-loop control. Four sensors with their electronics are integrated on one board with a length of 160 mm (Fig. 6); several boards can be connected together.

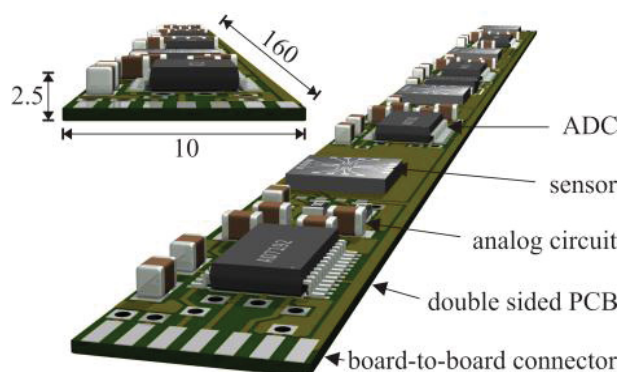


FIGURE 6. Pressure sensor board

The hot-film sensor is a microfabricated sensor to measure the wall shear stress and hence the flow velocity above the surface. The sensor contains a heating element, which dissipates heat to the ambient. The ability

to dissipate heat depends on the wall shear stress, so the temperature of the heated element adapts to it and hence the flow velocity and state. The sensing element adjusts its resistance to the temperature, so the output signal is given as an electrical resistance [11]. In contrast to hot-wire sensors the sensing element of a hot-film sensor is realized as a film directly deposited on a substrate. It has to be considered that this arrangement leads to a significant amount of heat dissipated by conduction into the substrate and further into the wing. In order to reach more detailed information about the flow in longitudinal and orthogonal direction, an array design with 32 hot-film sensors on one substrate is produced (FIG. 7) [12]. The sensor can be used in a closed-loop control which holds the temperature of the sensing element to a constant value (constant temperature anemometry). The current needed to hold the temperature gives a feedback about the wall shear stress on the sensor [12, 14].

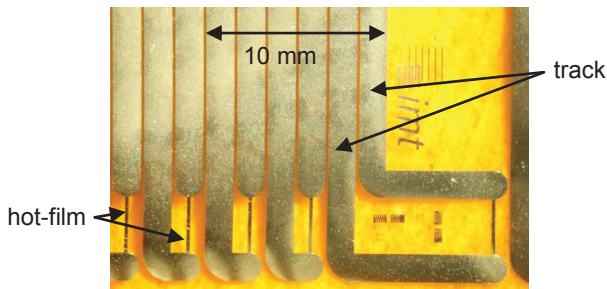


FIGURE 7. Micrograph of part of the hot-film array

Both sensors are measured and characterized after fabrication to evaluate their performance and check if the sensors are ready for use in the experimental setup. While the functionality for both sensors was shown using static tests, the dynamic characterization is still in progress. The pressure sensors were calibrated statically using a combined pressure and temperature chamber. In first tests the analog signal of the pressure sensor was amplified outside of the chamber. This relatively simple measurement method led to a high spreading of the results for constant temperature and pressure. Better results were achieved using the pressure sensor board (FIG. 6) inside the pressure chamber. Using this method, the output signal oscillates for +/- one bit when using a 16 bit analog-digital-counter, having constant pressure and temperature in the chamber. As mode of operation, the constant temperature anemometry is chosen, to achieve the lowest probability that the sensor burn-out due to overheating. The output signal is high- and low-pass-filtered to separate the average flow velocity and fast velocity changes (for example in turbulent flows). The results show both a dependency between low-pass-filtered signal and average velocity as well as turbulent responses in the high-pass-filtered-signal. This indicates that the functionality is given [13]. Detailed measurements to investigate the high frequency behavior are subject of present work.

4. STEPLESS LEADING EDGE DEVICE

In section two it was shown that a gapless leading edge device (droopnose) has the capability to greatly increase the performance and efficiency of a high lift system. The major challenges in the design of such a leading edge device lie in the design of a skin material for the wing that

allows the required deformation and the design of a compliant mechanism that is able to generate the required nose shape. Ways to address these challenges are presented in the following subsections.

4.1. Skin of a Contour Variable Droopnose

The crucial requirements for a morphing droop nose skin are the high formability due to bending in the airfoils chord direction. This, however, results in a small chordwise bending stiffness which must be compensated by a high spanwise bending stiffness. Most suggested morphing skins are primarily intended for in-plane morphing, e.g. zero-poisson honeycomb structures.

For the presented application, bending morphing skins are applied. Mainly two promising approaches are investigated. On one hand, corrugated laminates are considered with the aim to provide a preliminary design process for bending morphing applications, see [15, 16]. In order to conduct experiments of morphing skins with main application in bending deformation, a large bending test device is constructed, see [14]. It is based on a kinematic, which deviates from a pure state of bending by less than 0.2% up to a global bending curvature of 35 m^{-1} .

On the other hand, a hybrid skin structure consisting of compliant elastomer, combined with discrete fiber-reinforced stiff laminate bundles (FIG. 8) has been condensed out of various hybrid design variants.

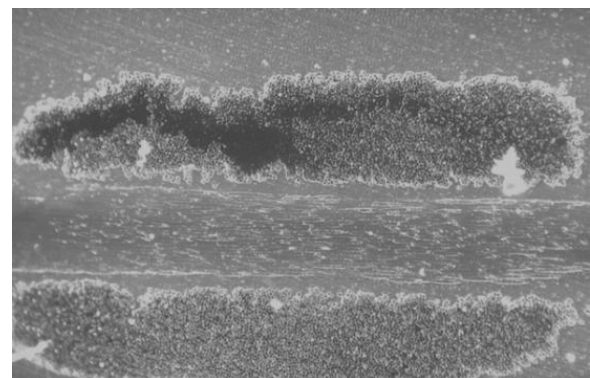
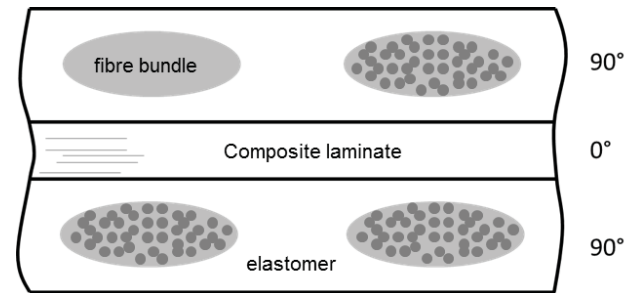


FIGURE 8. Sketch of the suggested hybrid skin structure (top) and polished micrograph section (bottom).

The functional principle of this structure is to avoid high strains within the discrete spanwise reinforcement. Instead, the majority of global bending strain is held by the elastomer in the outer regions. Thus, damage onset within the reinforcement bundles is significantly shifted to large global curvatures, see FIG. 9. Compared to fibres directly embedded in an elastomeric matrix this design shows considerably larger bending strength in spanwise direction.

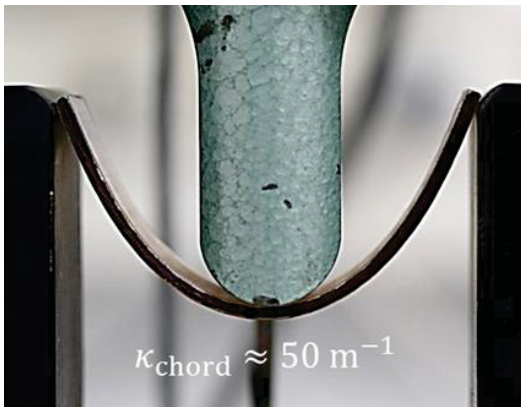


FIGURE 9. Static three-point bending test in chord (0°) direction

It should be mentioned that the design of the components of this material offers numerous degrees of freedom such as location and size of reinforcement bundles, elastomer stiffness and the design of the central composite laminate. Current manufactured configurations consisting of glass-fibre/epoxy and thermoplastic polyurethane show an outstanding ratio of spanwise to chordwise bending stiffness of around 15. Consequently, the ratio of anticlastic to morphing curvature is extremely small (0.0016) which is a key property with regard to shape integrity.

Due to the large number of design variables and large structural heterogeneity compared with the global deformation gradient, layer based homogenization techniques are limited. Thus, a numerical homogenization approach has been invented based on the representative volume element technique, see [16]. This approach is characterized by full 3D resolution of the structure with periodic boundary conditions working for in-plane as well as for bending deformation modes. Finally, representative stiffness properties in the sense of a full classical laminated plate theory are calculated.

4.2. Optimization of a Contour Variable Droopnose Structure

A skin material fit to match required bending and stiffness properties is on part of gapless leading edge device. The other important component is a compliant mechanism that is able to generate the required nose shape.

Although wing camber changing is widely used in commercial aircrafts to enhance their low speed capabilities, applied devices are mostly complex mechanical systems and are not able to provide a stepless aerodynamic shape. Therefore, the potential for improvement lies in a substitution of these systems by less complex gap- and stepless adaptive structures. Such kind of leading edge device was presented by Kintscher et al. in [17] and [18] as a result of the European project "Smart High Lift Devices for Next Generation Wings" (SADE) but the considered design reaches its limits in the degree of deflection of a conventional high lift system. An additional challenge is that a considerably higher level of morphing needed by the Coanda-flap based high lift system with circulation control presented by Burnazzi [4]. Apart from the previously addressed challenge to develop a skin that is flexible enough to sustain the desired shape change and is also stiff enough to carry the aerodynamic loads,

two other challenges arise concerning the morphing mechanism. (a) Design and creation of a morphing mechanism to transfer the actuator forces to the skin and aerodynamic loads to the wing structure; (b) Definition of an appropriate interface between the skin and the mechanism to provide the desired deformation according to the target shape. The focus of research lies in providing input for stiffness tailoring of the skin and the topology of the inner kinematics.

In the design process, optimization of the skin stiffness distribution is coupled to the optimization of the inner kinematics of the droopnose device, because these are parts of one elastic system and have decisive influence on the shape quality. Figure 10 shows the two-stage optimization framework which has been developed to determine skin stiffness distribution, topology of inner skin is shown giving the strain distribution of the material. Figure 11 illustrates the variation of skin thickness of the optimized skin [19]. With the ability to optimize the flexible skin, the developed framework is able to perform a topology optimization of the kinematic system. A topology optimization code, utilizing the SIMP approach presented by [20] and [21] was defined for nonlinear structures and implemented with a Globally Convergent Method of Moving Asymptotes (GCMMA) in MATLAB.

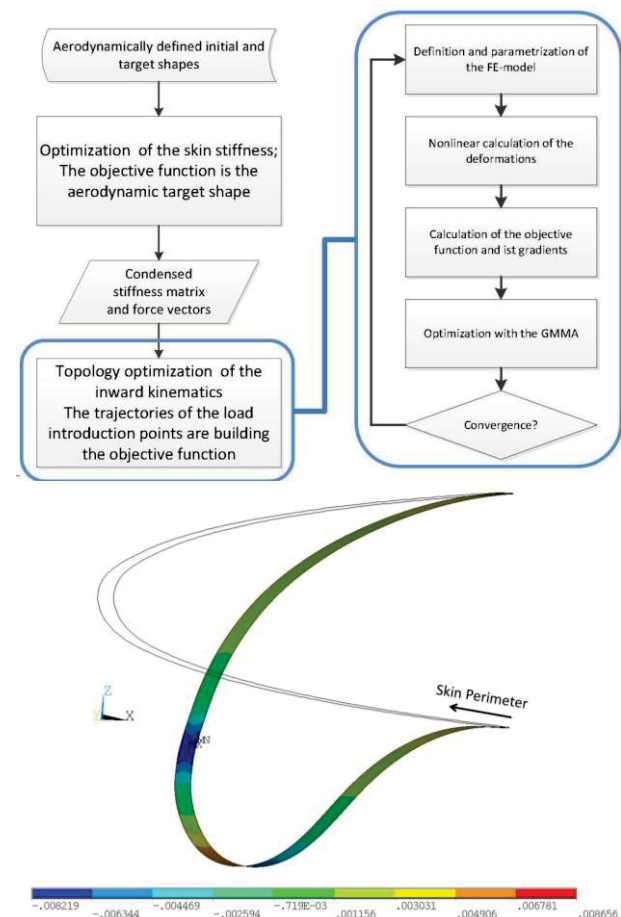


FIGURE 10. Optimization Process Chain with Preliminary Result of Deformation and Strain of the Leading Edge Skin in the High Lift Position

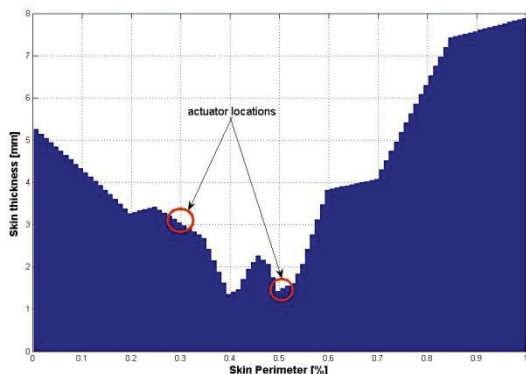


FIGURE 11. Preliminary Results of Variation of Skin Thickness

5. COMPACT COMPRESSOR SYSTEM

Complying with the modern concept of the all electric aircraft, a compact electrically powered compressor system is developed to provide the suction and blowing mass flow for the active lift system. One system provides the lift for each flap, located in the wing box between fuel tank and trailing edge flap. For cooling purposes, the electric motor is located in the inlet duct of the compressor (FIG. 12).

5.1. Compressor Design

The boundary conditions imposed by the high lift system require compressors with mass-flow rates from 0.6 kg/s – 2.5 kg/s at total pressure ratios from 1.3 – 2.3. Following an elementary design method for turbomachinery by Cordier [22], single stage axial compressors are found to be suited best for this operating range.

Due to advances in the research field of the external aerodynamics of the high lift system, the boundary conditions are subject to change during the project phase. To be able to relatively quickly redesign the compressor for the given boundary conditions of the lift system, an automated, optimized design process chain is developed. The optimization software CADO [23] based on meta-model assisted differential evolution is used.

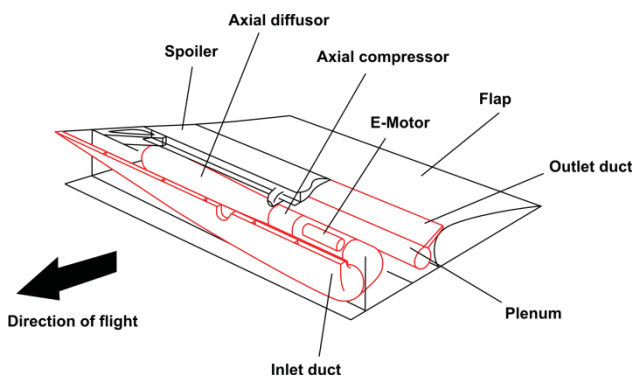


FIGURE 12. Compressor System in Wing Box

The optimized design process is separated into two phases illustrated in FIG. 13. After a conceptual design is fixed for the given boundary conditions, the major design parameters are determined using a preliminary design tools utilizing simplified physical models coupled with empirically based correlations. To investigate a wide range of parameters and also considering the complex

interaction between them, an automated optimization process is used. In this design phase, major design parameters are determined such as machine size, blade number, rotational speed, etc. Using simplified preliminary design tools these parameters can be determined efficiently without the need to determine detailed design parameters such as blade profile shape which require expensive detailed simulation.

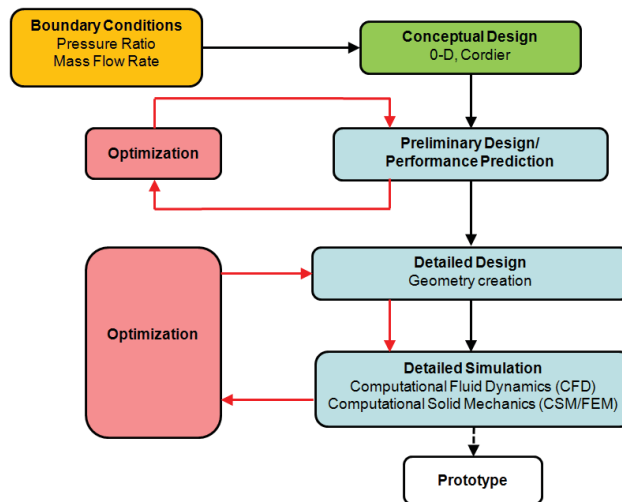


FIGURE 13. Optimization Design Process Chain for the Compressor Design

The used methodology and the results of the optimized preliminary design for a representative compressor of the high lift system are presented in [24], (FIG. 14).

With the major design parameters fixed, the design obtained in the preliminary design phase is then used as basis for further detailed design optimization. Here detailed machine parameters such as profile and blade shape are adjusted in order to match the required operating conditions. In the detailed design process not only aerodynamic performance but also structural integrity of the machine is a significant design objective.

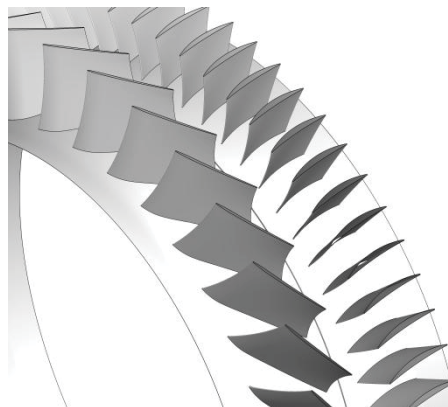


FIGURE 14. Result of optimized preliminary compressor design [24].

Separating the preliminary- and detailed design phase into different optimization processes offers the advantage of separating design parameters into groups of parameters of equal significance. This avoids a waste of optimization potential which occurs if the influence of machine parameters cannot be investigated due to the expensive

simulation or apparently insignificant, detailed parameters are omitted since basic machine parameters dominate it. In order to design an optimal electrical compressor system, the design process does not focus on the turbomachine alone but also needs to consider the interactions between the two systems compressor and electric motor. The implementation of these interactions in the optimized design process chain is subject to current work.

5.2. Electric Motor

The challenge of the electric motor design for this application lies in the high output power at high rotational speeds of up to 60,000 rpm. The motor is designed as a direct drive to avoid additional mechanical components.

From these boundary conditions several mechanical and electrical challenges arise. The main mechanical challenge is the high speed which leads to a high circumferential speed and thus limits the rotor diameter with respect to centripetal forces on the rotors surface [25]. Due to the limited maximum rotor diameter the machine length needs to be increased to achieve the required output power, thus decreasing the lateral critical speed. Compared to cage induction motors (IM), permanent magnet synchronous machines (PMSM) achieve a higher power density [26] and are therefore chosen for the motor design. The choice of the core material highly affects the motor's overall efficiency. Due to the necessary high ground frequencies, the magnetization losses make up to 83.5% of the overall losses by using standard core material. This requires the use of very thin core material to reduce eddy currents [27]. An effective dissipation of motor losses makes higher current densities in the stator winding possible, achieving higher power densities and lower motor weight. The highest power densities are reached with external cooling circuits, e.g. water cooling jackets. As an alternative, thermal analysis via lumped parameter model show that the in-line arrangement in Fig. 15 allows effective air cooling. The advantage compared to water cooling systems is lower complexity and an overall lower weight due to the fact that additionally pumps, pipes and fluids are not needed [27].

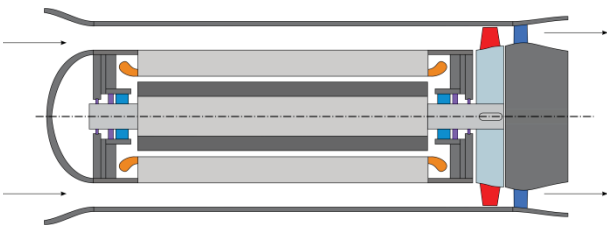


FIGURE 15. Motor integration in compressor concept

6. TURBOPROP INLET FOR STOL AIRCRAFT

The active lift system together with the goal of short take-off and landing (STOL) capabilities of the reference aircraft require increased performance of the turboprop engines.

One field of research is to provide design guidelines for the inlet component of the turboprop engine for the reference aircraft. While meeting the aerodynamic specifications of a turboprop, the inlet has to provide uniform mass flow in all mission phases including STOL. In this phase, a high thrust level of the engine is required

due to the high-lift feature of the reference aircraft. Since the aircraft has been sized for a tractor type turboprop, the inlet geometry requires an S-shaped diffuser. Therefore, the objective of this work is to develop a parametric design method of an S-shaped inlet and to analyze the flow in order to investigate the distortion effects at the aerodynamic interaction plane (AIP). Additional challenges are the consideration of the propeller interaction for highly loaded, high speed propeller, the power demand of the high-lift system and wing installation effects of the engine. Different inlet characteristics such as scoop type, boundary layer diverter (BLD) and integrated particle separator (IPS) are investigated. Consequently this research also addresses the conceptual design of the turboprop engine. This is necessary in order to accurately estimate the engine size and to provide a realistic approach of the inlet flow effects on aerodynamic efficiency. To investigate the effect of high power demand on aerodynamic efficiency and performance, inlets for three engine concepts are compared. The inlet design is chosen as single scoop, shaft penetration configuration with a conventional spread angle as described in [28]. The reference geometry is further simplified by equating the scoop width and inlet exit diameter and excluding the IPS (FIG. 16).



FIGURE 16. Generic inlet concept for aerodynamic analysis

The turboprop conceptual design is defined as a 2-spool axial compressor configuration based on the results of [29]. The basis turboprop engine is designed without the high-lift requirement using the commercially available software package GasTurb 12. Two possible engine concepts which can support the high-lift system are designed. One engine design supplies air for the Coanda flap using a conventional engine bleed air system and the other engine concept provides additional shaft power to a generator to power the compressor systems. The inlet area increases by 50% compared to the reference engine when high-lift system is supplied with air flow from the core engine mass flow. The additional power supply concept introduces only a 20% increase in the inlet area compared to the reference engine (FIG. 17).

The next steps in this project focus on the design of the inlet of the power supplying turboprop concept. For this design the inlet area increase is less than the bleed air concept. The overall inlet geometry is varied to observe the sizing effects. The internal flow analysis results will then be used to enhance the inlet geometry for efficient pressure recovery and flow uniformity.

Also as a comparison case, contemporary turboprop inlets with similar configuration choices will be used. Even though the inlet configuration for high speed turboprop applications has been studied since four decades [30], the

current number of applications is small compared to turbofan powered examples. The examples are limited when the high thrust level is also considered. The most similar and recent case is Airbus A400M's TP400 turboprop engine, which delivers around 8 MW take-off power and provides a cruise speed of Mach 0.72. It has an offset gearbox configuration with pinion low arrangement [31], therefore uses an S-shaped diffuser with a wide scoop spread angle. A representative inlet geometry based on this engine [32] is modeled and included into the solution procedure.

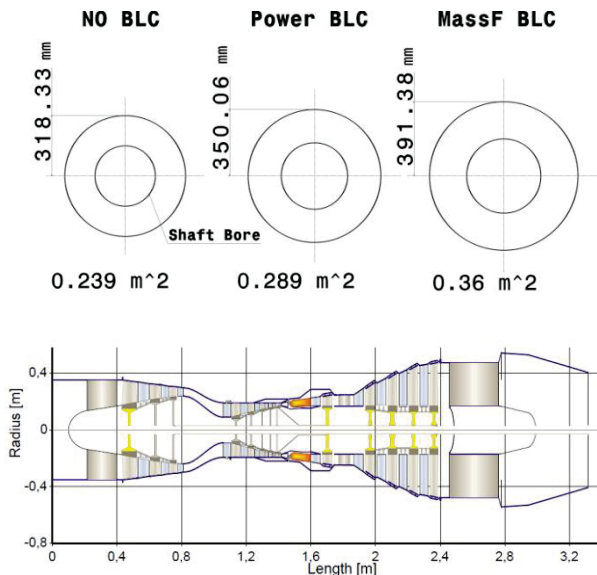


FIGURE 17. Conceptual engine design

7. CONCLUSIONS

The present paper summarizes the research results in the field of efficient high lift as part of the collaborative research center (SFB) 880. It is shown that the efficiency of an active high lift system utilizing Coanda flap blowing and wall suction. With these methods, the required jet momentum to achieve the target lift coefficient can be reduced by 40%. The methodologies chosen to model and develop a closed-loop control of the blowing system are presented. In order to actuate the lip which controls the blowing, piezo ceramic actors are developed and implemented in a model for water tunnel testing. A non-intrusive sensor system which is embedded in the wing and flap is developed. The sensor system relies on piezo-resistive sensors to detect pressure and hot-film sensors to detect velocity. The fundamentals of the skin material and the compliant mechanism for a gapless and stepless droopnose are researched. To allow flexibility in chordwise direction and stiffness in spanwise direction, circular corrugated composites are investigated. To predict the deformation limits of these materials, models are developed and validated through experimental testing. To determine the required stiffness distribution and the topology of the compliant mechanism for achieving the required droopnose shape for all significant flight conditions, an optimization framework is developed. Using synergy effects, compressor systems are developed for each flap to supply the suction and blowing air mass flow rate of the lift system. Following the concept of the all-

electric aircraft these compressors are electrically powered. An optimized design-process chain for the compressors is developed. An electric motor that achieves the required high power output at high rotational speeds was designed. To provide cooling to the motor, it is located in the inlet duct of the compressor. The increased thrust, as well as the required power of the lift system requires turboprop engines with increased power. Studies of the compressor inlet design of this engine as well as conceptual designs of the engine are presented. It is shown that an engine which does not supply electrical power to the lift system but instead supplies the air mass flow through an engine bleed system directly has a prohibitively larger intake area.

8. ACKNOWLEDGMENTS

Funding for this work is provided by the German Research Foundation DFG through the collaborative research center (SFB) 880 "Fundamentals of High Lift for Future Civil Aircraft". The authors would like to thank everyone involved in presented research.

REFERENCES

- [1] Jensch, C., Pfingsten, K. C., Radespiel, R., Schuermann, M., Haupt, M., and Bauss, S.: Design Aspects of a Gapless High-Lift System with Active Blowing, DLRK 2009, Aachen, 2009.
- [2] Jensch, C., Pfingsten, K. C., and Radespiel, R.: Numerical Investigation of Leading Edge Blowing and Optimization of the Slot and Flap Geometry for a Circulation Control Airfoil, Notes on Numerical Fluid Mechanics and Multidisciplinary Design, Vol. 112, Springer Verlag, 2010.
- [3] Pfingsten, K. C., Jensch, C., Körber, K. V., and Radespiel, R.: Numerical simulation of the flow around circulation control airfoils, First CEAS European Air and Space Conference, Berlin, 2007.
- [4] Burnazzi, M, and Radespiel, R.: Design of a Droopnose Configuration for a Coanda Active Flap Application, 51th AIAA Aerospace Sciences Meeting, Dallas (TX), AIAA 2013-0487.
- [5] Liu, Y., Sankar, L. N., Englar, R., J., and Ahuja, K., K.: Numerical Simulations of the Steady and Unsteady Aerodynamic Characteristics of a Circulation Control Wing Airfoil, 39th AIAA Aerospace Sciences, Meeting & Exhibit, AIAA Paper 2001-0704.
- [6] Noack, B., R., Afanasiev, K., Morzynski, M., Tadmor, G., and Thiele, F.: A hierarchy of low-dimensional models for the transient and post-transient cylinder wake, Journal of Fluid Mechanics, 497, 335–363, Cambridge University Press, 2003.
- [7] Luchtenburg, D., M., Günther, B., Noack, B., R., King, R., and Tadmor, G.: A generalized mean-field model of the natural and high-frequency actuated flow around a high-lift configuration, Journal of Fluid Mechanics, 623, 283–316, Cambridge University Press, 2009.
- [8] Bergmann, M., Cordier, L., and Brancher, J., P.: Optimal rotary control of the cylinder wake using proper orthogonal decomposition reduced-order model, Physics of Fluids, 17, 097101, 2005.
- [9] Cordier, L., Abou El Majd, B., and Favier, J.: Calibration of POD reduced order models using Tikonov regularization, International journal for numerical methods in fluids, 63, 569–296, 2010.

- [10] Beutel, Tobias, Leester-Schädel, Monika and Büttgenbach, Stephanus. Design and evaluation process of a robust pressure sensor for measurements in boundary layers of liquid fluids. *Microsystem Technologies*, Springer-Verlag, August 2012. Vol. 18, Issue 7-8, pp. 893-903. DOI 10.1007/s00542-011-1404-x.
- [11] Eckelmann, Helmut. *Einführung in die Strömungsmeßtechnik*. s.l. : Teubner Verlag, 1997. ISBN: 3-519023792.
- [12] Beutel, Tobias, Leester-Schädel, Monika and Dietzel, Andreas. Design and Manufacturing of Flexible Micro Hot Film Probes for Aeronautical Purposes. *Mikro- and Nanoengineering*. Toulouse, France : s.n., 2012.
- [13] Beutel, Tobias, et al. Flexible Hot-film Anemometer Arrays for Flow Measurements on Curved Structures. *Microsystem Technologies*. May 17, 2013. Vol. 18, Issue 7-8, pp. 893-903. DOI 10.1117/12.2016755.
- [14] Schmitz A, Horst P. Bending deformation limits for corrugated morphing skins. ICCM19 Montréal 2013; 8942-8950.
- [15] Schmitz A, Horst P. Bending deformation limits of corrugated unidirectional reinforced composites. *Composite Structures* 2013; doi:10.1016/j.compstruct.2013.07.048.
- [16] Schmitz A, Horst P. Numerical modelling of the change in stiffness properties of cross-ply laminates subjected to large bending curvatures. *Key Engineering Materials* 2014; 577-578:173-176.
- [17] Kintscher, M., Wiedemann, M. (2012). Design of a smart leading edge device. *Adaptive, Tolerant and Efficient Composite Structures* Springer. 381-390. ISBN 978 3 642 29189 0
- [18] Kintscher, M., Wiedemann, M., Monner, H.P., Heintze, O., Kühn, T. (2011) Design of a smart leading edge device for low speed wind tunnel tests in the European project SADE. *International Journal of Structural Integrity* vol. 2, 4, 383-405
- [19] Sigmund, O. (1997) On the Design of Compliant Mechanisms Using Topology Optimization. *Mechanics of Structures and Machines: An International Journal*, 25:4, 493-524
- [20] Bendøe, M., Sigmund, O. (2004) *Topology Optimization Theory, Methods and Applications* ISBN 3 540 42992 1
- [21] Rudenko A., Rose, M. Optimization framework for stiffness and layout tailoring of a morphing high lift system, 6th ECCOMAS Thematic Conference on Smart Structures and Materials (SMART2013)
- [22] Grote, K.-H., Feldhusen, J. (2007) *Dubbel - Maschenbuch für den Maschinenbau*, 22. Auflage, Springer Verlag, Berlin
- [23] Verstraete, T. (2010) CADO: a Computer Aided Design and Optimization Tool for Turbomachinery Applications, 2nd International Conference on Engineering Optimization, Lisbon, Portugal
- [24] Teichel, S. et.al (2013) Optimized preliminary design of compact axial compressors: A comparison of two design tools, 31st AIAA Applied Aerodynamics Conference June 24-27, 2013, San Diego, CA
- [25] Binder, A, Schneider, T., Klohr, M. (2005) Fixation of buried and surface mounted magnets in high-speed permanent magnet synchronous motors, Conference Record of the 2005 Industry Applications Conference, 2843-2848
- [26] Soong, W.L., Kliman, G.B., Johnson, R.N., White, R.A., Miller, J.E. (2000) Novel high-speed induction motor for a commercial centrifugal compressor, *IEEE Transactions on Industry Applications*, 36(3), 706-713.
- [27] Dörbaum, M, Juris, P, Stübig, C, Ponick, B (2013) Design of High Speed Motor with a High Power Range for Use in Future Aircrafts, PCIM Europe, Nürnberg
- [28] Hancock, J.P., et al., Analysis of Results from Wind Tunnel Tests of Inlets for an Advanced Turboprop Nacelle Installation, NASA-CR-74937, 1986
- [29] Reynolds, C.N., *Advanced Propfan Technology*, NASA-CR-168114-V1, 1985
- [30] Whitlow, J.B., Sievers, G.K., Fuel Savings Potential of the NASA Advanced Turboprop Program, NASA TM-83736, 1984
- [31] Little Jr., B.H., Propulsion System Installation Design for High-Speed Prop-Fans, *Journal of Aircraft*, Vol. 20, No. 5, 1983
- [32] Gaertner, W., Development-Share of MTU Aero Engines in TP400-D6, Propulsion-System for A400M, ISABE-2005-1166